Approaching Ideal Visibility in Singlet-Triplet Qubit Operations Using Energy-Selective Tunneling-Based Hamiltonian Estimation

Jehyun Kim,[1,†] Jonginn Yun,[1,†] Wonjin Jang,[1,†] Hyeongyu Jang,[1] Jaemin Park,[1] Younguk Song,[1] Min-Kyun Cho,[1] Sangwoo Sim,[1] Hanseo Sohn,[1] Hwanchul Jung,[2] Vladimir Umansky,[3] and Dohun Kim[1,*]

[1]*Department of Physics and Astronomy, and Institute of Applied Physics, Seoul National University, Seoul 08826, Korea*
[2]*Department of Physics, Pusan National University, Busan 46241, Korea*
[3]*Braun Center for Submicron Research, Department of Condensed Matter Physics, Weizmann Institute of Science, Rehovot 76100, Israel*

(Received 1 March 2022; revised 15 May 2022; accepted 28 June 2022; published 19 July 2022)

We report energy-selective tunneling readout-based Hamiltonian parameter estimation of a two-electron spin qubit in a GaAs quantum dot array. Optimization of readout fidelity enables a single-shot measurement time of 16 μs on average, with adaptive initialization and efficient qubit frequency estimation based on real-time Bayesian inference. For qubit operation in a frequency heralded mode, we observe a 40-fold increase in coherence time without resorting to dynamic nuclear polarization. We also demonstrate active frequency feedback with quantum oscillation visibility, single-shot measurement fidelity, and gate fidelity of 97.7%, 99%, and 99.6%, respectively, showcasing the improvements in the overall capabilities of GaAs-based spin qubits. By pushing the sensitivity of the energy-selective tunneling-based spin to charge conversion to the limit, the technique is useful for advanced quantum control protocols such as error mitigation schemes, where fast qubit parameter calibration with a large signal-to-noise ratio is crucial.

DOI: 10.1103/PhysRevLett.129.040501

The efficient and precise characterization of a quantum system is important for building scalable quantum technologies that are robust to noise stemming from a fluctuating environment [1,2]. Estimating Hamiltonian parameters faster than the characteristic noise fluctuation timescale is essential, where knowledge gained from the measurement is used for correcting control parameters [2–4]. Active measurement-based feedback, for example, is used to enhance quantum sensing [5,6]. For semiconductor quantum dot (QD)-based spin qubit platforms, Hamiltonian parameter estimation applied to GaAs has shown that the effect of quasistatic nuclear spin fluctuation can be strongly suppressed for both single spin [7] and singlet-triplet qubits [2]. While the development of spin qubits in nuclear noise-free group-IV materials such as ^{28}Si shows impressive progress in increasing single spin qubit coherence times [8,9], two-qubit control fidelity is often impeded by charge noise, which is also often sufficiently non-Markovian [10] and hence suppressible. Thus, fast Hamiltonian learning methods are expected to be used for a wide range of materials in noisy intermediate-scale quantum systems.

The fast single-shot measurement of qubits with high fidelity is a prerequisite for enabling Hamiltonian estimation. Semiconductor spin qubit devices mostly utilize a nearby charge sensor, where spin states are distinguished via spin to charge conversion mechanisms such as energy-selective tunneling (EST) [11,12] or Pauli spin blockade (PSB) [13]. While both mechanisms are applicable for the detection of single spin [11], singlet-triplet (ST_0) [13], and exchange only qubits [14], PSB-based readout has been predominantly used for real-time Hamiltonian estimation owing to its deterministic readout time and fast initialization capability [15]. However, direct application of PSB often suffers from small signal contrast due to suboptimal sensor position relative to double quantum dot (DQD) or fast relaxation at the readout condition due to large magnetic field difference-induced singlet state tunneling or the effect of spin-orbit coupling [16]. Variants of PSB-based readout have been developed using electron latching mechanisms in sufficiently isolated quantum dots [17,18] or by mapping to states outside the qubit space [19] circumventing some of the PSB-readout's known disadvantages. For Si devices, high readout visibility has been demonstrated using both PSB and EST readout owing to relatively long relaxation time [20–22]. However, so far the experiments using GaAs devices showed visibility below 80% using PSB readout.

The EST-based single-shot readout, on the other hand, guarantees a signal contrast corresponding to a full electron charge and long relaxation time [23,24]. As the Hamiltonian learning efficiency is directly affected by the ideality of the likelihood function, the large signal-to-noise ratio (SNR) of the EST readout can potentially be used for real-time Hamiltonian parameter estimation. Because the EST readout suffers from the intrinsically probabilistic nature of electron tunneling, requiring a longer waiting time than the PSB readout [25], it is important to determine whether the current state-of-the-art sensitivity of the rf-charge sensor can provide an EST readout that is sufficiently fast and

simultaneously has a large SNR to enable efficient qubit frequency estimation on the fly.

In this Letter, we demonstrate real-time Hamiltonian parameter estimation by EST-based single-shot readout with sub-MHz accuracy in qubit frequency verified by observing over a 40-fold increase in coherence time T_2^* compared to that of bare evolution on the order of 20 ns in GaAs [13]. With frequency feedback, the single-qubit operation performance in terms of initialization, manipulation, and measurement fidelity is one of the best figures reported thus far for semiconductor spin qubits, providing a promising route for applying the EST-based single-shot readout method to various qubit operations.

The quantum system we study is an ST_0 qubit with a basis state singlet $|S\rangle$ and triplet-zero $|T_0\rangle$, formed by two gate-defined lateral QDs. Figure 1(a) shows a scanning electron microscope image of a quantum dot device similar to the one we measured. Au/Ti gate electrodes were deposited on top of the GaAs/AlGaAs heterostructure, where a 2D electron gas is formed 70 nm below the surface. Focusing on the DQD denoted by green circles in Fig. 1(a), high-frequency voltage pulses combined with dc voltages through bias tees are input to gates V_1, V_2, and V_M. rf reflectometry was performed by injecting a carrier frequency of ≈125 MHz with an estimated power of −100 dBm at the Ohmic contacts and monitoring the reflected power through homodyne detection. The device was operated in a dilution refrigerator with base temperature ≈ 7 mK and with an external magnetic field H_{ext}. The measured electron temperature is ≈72 mK [26–28].

The qubit Hamiltonian is given by $H = [J(\varepsilon)/2]\sigma_z + (\Delta B_z/2)\sigma_x$, where $J(\varepsilon)$ is the exchange splitting between states $|S\rangle$ and $|T_0\rangle$ controlled by potential detuning ε, $\sigma_{i=x,y,z}$ is the Pauli matrix, and ΔB_z is the magnetic field difference between QDs set by the hyperfine interaction with the host Ga and As nuclei. We adopted units where $g^*\mu_B/h = 1$, in which $g^* \approx -0.44$ is the effective gyromagnetic ratio in GaAs, μ_B is the Bohr magneton, and h is Planck's constant. With the quantum control provided by rapidly turning on and off $J(\varepsilon)$, the main task is to estimate ΔB_z, which varies randomly in time owing to statistical fluctuations of the nuclei. The basic idea of the Bayesian inference is to update one's knowledge about the Hamiltonian parameter by comparing the measurement results with the expected form of time evolution (likelihood function). Based on the single-shot projective measurement of the qubit evolving around the x axis on the Bloch sphere for time $t_k = 4k$ ns (Larmor oscillation), Bayesian inference is performed by the following rule up to a normalization constant [2]:

$$P(\Delta B_z|m_N, m_{N-1}, \ldots, m_1) = P_0(\Delta B_z)\prod_{k=1}^{N}\frac{1}{2}\{1 + r_k[\alpha + \beta\cos(2\pi\Delta B_z t_k)]\}, \quad (1)$$

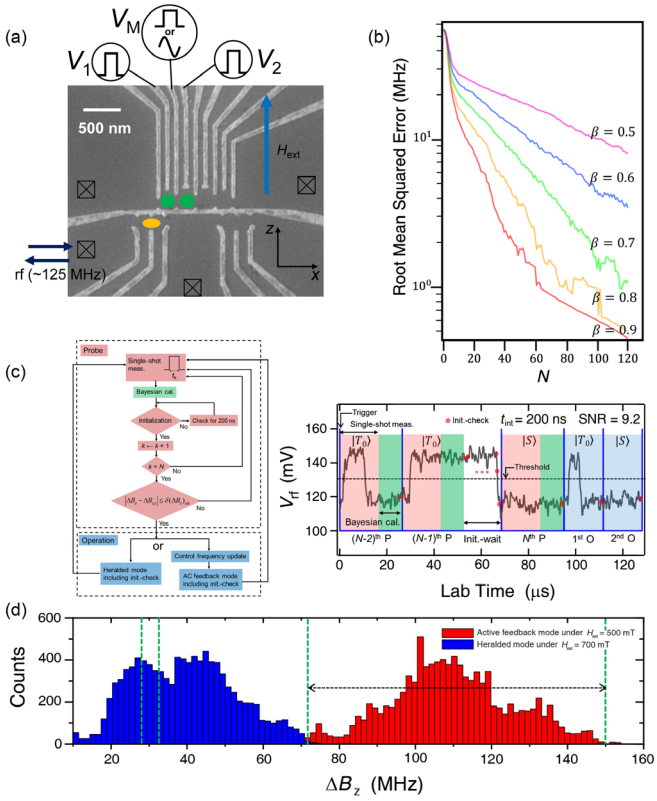

FIG. 1. (a) Scanning electron microscopy image of a device similar to the one used in the experiment. Green (yellow) circles indicate the position of quantum dots for the ST_0 qubit (rf charge sensor). H_{ext} is applied to the z axis as indicated by the blue arrow. (b) Root mean squared error of the Bayesian estimator as a function of N and β. (c) Left panel: block diagram of the experimental procedure including the probe and operation step, where the latter is performed either in heralded or active feedback mode. Right panel: example scope trace of the charge sensor signal recorded during the experiment. Gray trace: rf-demodulated sensor signal with SNR = 9.2 at $t_{\mathrm{int}} = 200$ ns. Blue trace: trigger signals marking the start timings of each probe and operation step. The red dots show the timings of the initialization check sequences. (d) Histograms of ΔB_z obtained by running the probe step 10 000 times at two different H_{ext}. For the heralded (active feedback) mode, $\delta(\Delta B_z)_{\mathrm{set}}$ on the order of 1 MHz (few tens of MHz) around an average ΔB_z of 30 (110) MHz was chosen. Green dashed lines indicate a tolerance window $2\delta(\Delta B_z)_{\mathrm{set}}$.

where N is the number of single-shot measurements per Hamiltonian estimation, $P_0(\Delta B_z)$ is the uniform initial distribution, $r_k = 1(-1)$ for $m_k = |S\rangle(|T_0\rangle)$, and $\alpha(\beta)$ is the parameter determined by the axis of rotation (oscillation visibility). After the Nth single-shot measurement and update, the most probable ΔB_z is determined from the posterior distribution $P(\Delta B_z|m_N, m_{N-1}, \ldots, m_1)$.

In the likelihood function $\frac{1}{2}\{1 + r_k[\alpha + \beta\cos(2\pi\Delta B_z t_k)]\}$, ideally, $\alpha = 0$ and $\beta = 1$. Figure 1(b) shows the simulation results of the root mean squared error between the true and estimated ΔB_z. Compared to the low-visibility case ($\beta = 0.5$) corresponding to a large measurement error, the

high-visibility case ($\beta = 0.9$) shows a large improvement in the rate of convergence, reaching submegahertz accuracy in less than $N = 70$. To date, Bayesian estimations of quantum dot spin qubits have been performed with $\beta \sim 0.7$ [2,7] requiring $N > 120$ for practical Hamiltonian estimation. Below, we show that the EST readout indeed provides β reaching unity enabling efficient frequency detection and feedback.

Figure 1(c) shows a schematic block diagram and an example scope trace during the experiment. We set the integration time of the rf demodulator $t_{\rm int} = 200$ ns, at which SNR $= 9.2$ [15,24,26,29–32]. The measurement time was set to 15 μs, during which the dot-to-reservoir tunnel rate tuned to the order of 1 MHz ensures that a tunnel-out event occurs for the state $|T_0\rangle$. For the probe sequence, we diabatically pulse ε to rapidly turn off J. The calculation time according to Eq. (1) is $\approx$10 μs after the kth measurement. For the operation, there are two types of modes. The first is a heralded mode where the operation is conditionally triggered only when the estimated qubit frequency in the probe step falls within a preset tolerance $\delta(\Delta B_z)_{\rm set}$ around the target frequency $\Delta B_{z,t}$. Once a short operation on the order of 20 shots is finished, one has to wait for the next $\Delta B_{z,t} \pm \delta(\Delta B_z)_{\rm set}$ to happen. The method is conceptually similar to Ref. [37] where the Bayesian estimator-based heralding was used to effectively suppress thermally induced initialization error. The second is the active feedback mode where resonant modulation of $J(\varepsilon)$ (Rabi oscillation) is performed using the frequency obtained from the probe step. Here, $\delta(\Delta B_z)_{\rm set}$ is typically set to more than 70 MHz and the control frequency is actively adjusted so that the waiting time is minimized. In all steps, we apply an adaptive initialization step [37,38] where the controller triggers the next experiment provided that the state is $|S\rangle$. Including all the latency components, the repetition period for one probe (operation) step is approximately 26(16) μs on average [26]. Figure 1(d) shows typical histograms of ΔB_z obtained by repeatedly running the probe step at different $H_{\rm ext}$, showing fluctuation about a nonzero mean ΔB_z. Note that the average ΔB_z depends on $H_{\rm ext}$. While the exact origin of this is not well understood to date, previous studies in GaAs quantum dot report similar behavior [39,40], and we adjust $H_{\rm ext}$ to set the most probable ΔB_z about 30 MHz (110 MHz) for the heralded (active feedback) mode.

First, we demonstrate the performance of the EST-based Bayesian estimator using the heralded mode operation. Figure 2(a) shows the representative Larmor oscillations where P_1 is the triplet return probability with $N = 70$, $\Delta B_{z,t} = 30$ MHz, and $\delta(\Delta B_z)_{\rm set} = 0.1$ MHz. The measurement of $T_2^*(N)$, extracted by fitting the Larmor oscillations to a Gaussian decay, reveals the uncertainty of the EST-Bayesian estimation [Fig. 2(b)]. The initial increase in $T_2^*(N)$ corresponds to an improvement in the estimation accuracy. T_2^* reaches an optimal coherence time of over

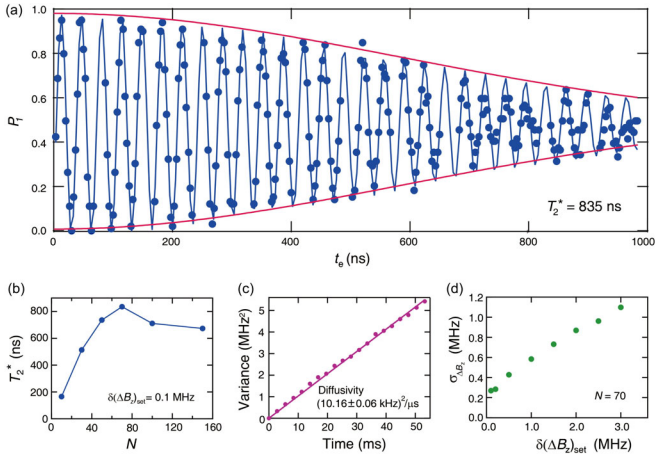

FIG. 2. (a) Representative Larmor oscillations with $N = 70$ showing $T_2^* = 835$ ns, with a fit to a Gaussian decay function (red envelope and blue oscillatory fit). (b) T_2^* as a function of N, showing an optimal $N = 70$ with $\delta(\Delta B_z)_{\rm set} = 0.1$ MHz. (c) The variance of the ΔB_z as a function of elapsed time showing a diffusion process with the diffusivity $(10.16 \pm 0.06\ {\rm kHz})^2/\mu$s. (d) The uncertainty of the frequency estimation $\sigma_{\Delta B_z}$ as a function of the half-width of the tolerance $\delta(\Delta B_z)_{\rm set}$.

800 ns near $N = 70$ and subsequently decreases for $N > 80$. The latter reflects the effect of nuclear fluctuation during the increased estimation period consistent with the diffusive behavior of ΔB_z with diffusivity $D = 10.16\ {\rm kHz}^2/\mu$s [Fig. 2(c)] [2].

Figure 2(d) shows the $\delta(\Delta B_z)_{\rm set}$ dependence of the experimental estimation uncertainty $\sigma_{\Delta B_z} = 1/\sqrt{2}\pi T_2^*$ [41]. As we set the tolerance more stringently [smaller $\delta(\Delta B_z)_{\rm set} = 0.1$ MHz], T_2^* increases correspondingly. The residual uncertainty of the EST-based Bayesian estimator when $\delta(\Delta B_z)_{\rm set} = 0$ is approximately 0.25 MHz. It is likely overestimated by the nuclear fluctuation during the operation time of 0.32 ms (16 μs $\times$ 20 shots) after the probe step. Thus, we conclude that our Hamiltonian estimation scheme enables qubit frequency estimation in 70 shots with an accuracy better than 0.25 MHz. Note also that while the maximum $T_2^* = 835$ ns we observe is less than the PSB-based Hamiltonian estimation [2], the actual performance of the PSB and EST-based Bayesian estimators is difficult to directly compare so far because the dynamic nuclear polarization [3,42] is not used in the current experiment.

We now discuss the application of the EST-based Hamiltonian estimation to general single-qubit operations (Fig. 3, heralded mode; Fig. 4, active feedback mode). Figure 3(a) shows coherent Larmor oscillations with $\Delta B_{z,t} = 30$ MHz. The oscillation shows the visibility of approximately 97.7%. Considering possible imperfections in the control stemming from residual J and finite rise time of the waveform generator ($\sim$0.4 ns), the result shows that the EST-based Bayesian method enables accurate qubit

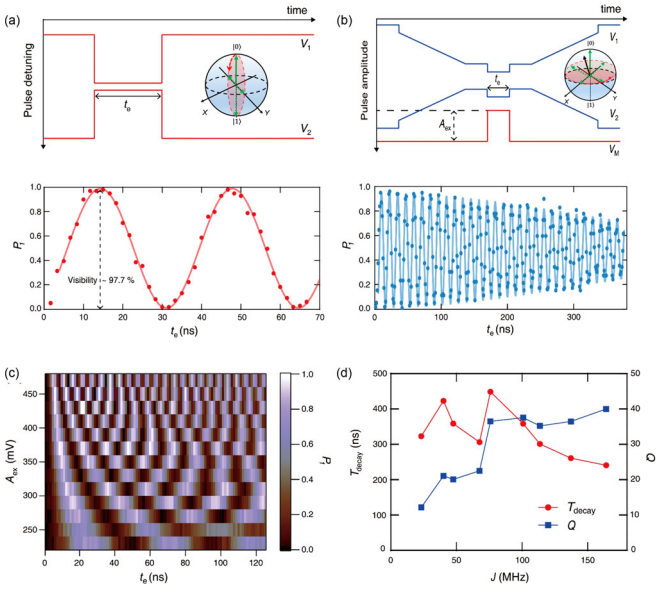

FIG. 3. (a) Top: Pulse sequences applied to gates V_1 and V_2 for the heralded Larmor oscillations measurement. Bottom: Larmor oscillations with visibility higher than 97%. (b) Top: Pulse sequence for coherent exchange operation. Bottom: Corresponding exchange oscillations at $J = 75$ MHz, $\Delta B_{z,t} = 30$ MHz showing charge noise-limited coherence time $T_{\mathrm{decay}} = 450$ ns. (c) Exchange oscillations as a function of barrier pulse amplitude A_{ex} and evolution time t_e. (d) T_{decay} and the quality factor Q as a function of exchange coupling J.

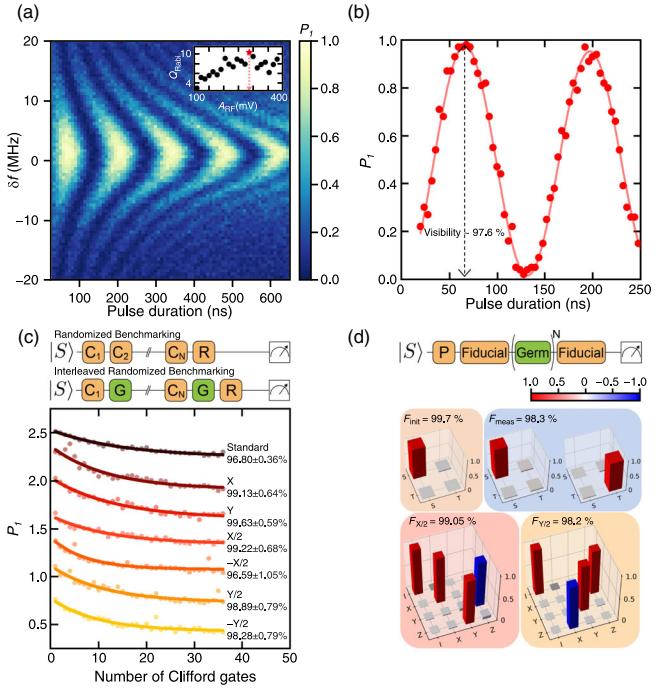

FIG. 4. (a) Rabi oscillation of P_1 as a function of controlled detuning δf and pulse duration. Inset: Oscillation quality factor Q_{Rabi} as a function of rf amplitude A_{rf} (measured at the output of the signal generator). The red symbol marks the condition for the maximum Q_{Rabi}. (b) Representative Rabi oscillation with visibility higher than 97%. The oscillation is fit to the sinusoidal function with the Gaussian envelope, from which Rabi decay time $T_{\mathrm{Rabi}} = 1.71$ μs is obtained. (c) P_1 as a function of the number of random Clifford gates obtained from a single qubit standard and interleaved randomized benchmarking. Traces are offset by 0.3 for clarity. (d) Density matrices (top row) and Pauli transfer matrices (bottom row) evaluated by gate set tomography.

frequency estimation and high measurement fidelity at the same time, leading to near ideal visibility. By comparing the oscillation with the numerical simulation, we estimate measurement fidelity of 99% with less than 0.1% initialization errors for the heralded mode [23,26,33,34].

Using symmetric barrier-pulse operation, recently demonstrated in Ref. [43], Fig. 3(b) shows coherent exchange oscillations with $\Delta B_{z,t} = 30$ MHz, and $J = 75$ MHz. In addition, a two-dimensional map of the exchange oscillations is measured as a function of exchange amplitude A_{ex} and exchange duration t_e [Fig. 3(c)], showing the oscillations with a high-quality factor Q. Moreover, $Q(J)$ follows the general trend observed in previous results [43] where Q (T_{decay}) tends to saturate (decrease) at large J owing to the crossover from nuclear noise to electrical noise-limited decoherence. While the maximum Q of ~40 is comparable to that in the previous report [43], our EST-based Bayesian method effectively suppresses the ΔB_z fluctuation, leading to the observation of $Q > 30$ in a wide range of J.

Although the heralded mode operation exemplifies the performance of the EST-based Hamiltonian estimator with minimal overhead in the Bayesian circuit, the main drawback is the low duty cycle (actual operation time divided by waiting time), which can be <1% depending on the tolerance. Thus, we further develop our methodology using ac-driven qubit operation in active feedback mode. The pulse sequence for qubit operation is the same as in Fig. 3(b) except that a sinusoidal rf pulse is applied to V_M using the frequency detected in the probe step. In this manner, the total waiting time is reduced down to one probe step (70 shots × 26 μs = 1.82 ms). Figure 4(a) shows the coherent Rabi oscillation measured as a function of the rf pulse duration and controlled detuning δf. The pulse amplitude A_{rf} is chosen to maximize the Q factor $Q_{\mathrm{Rabi}} = f_{\mathrm{Rabi}} T_{\mathrm{Rabi}} \approx 12$ with the Rabi frequency f_{Rabi} of 6.05 MHz and the Rabi decay time T_{Rabi} of 1.71 μs [inset to Fig. 4(a)]. The oscillation visibility reaches approximately 97.6%, [Fig. 4(b)]. This near-ideal visibility of the rf-driven oscillation even without dynamic nuclear polarization again reveals the precise qubit frequency estimation and high measurement fidelity simultaneously enabled by the EST-based Bayesian estimator.

Furthermore, we perform the standard randomized benchmarking (RB) and interleaved randomized benchmarking (IRB) where single-qubit gates X, Y, $X/2$, $Y/2$, $-X/2$, and $-Y/2$ are interleaved to random Clifford gates [35,44,45]. The recovery gate is chosen such that the final state is ideally

singlet, and the gate fidelity is obtained by fitting the measured data to the exponentially decaying curve [26,35]. We find the average gate fidelity F_{avg} of 96.80% and π-pulse fidelity F_X of 99.13%, the latter being close to the Q-factor limited value $e^{-1/(2Q_{\mathrm{Rabi}})^2} = 99.76 \pm 0.03\%$.

To compare the state preparation and measurement (SPAM) errors between two operation modes, we perform gate-set tomography (GST) [34]. Figure 4(d) shows the density matrix (top row) and the Pauli transfer matrix (PTM, bottom row), obtained using a single qubit GST protocol with a gate set {I, $X/2$, and $Y/2$} [26,36], from which we obtain $F_{X/2} = 99.05\%$ and $F_{Y/2} = 98.2\%$, consistent with the values obtained from the IRB. The GST yields the initialization fidelity of 99.7% and measurement fidelity of 98.3%. We ascribe slightly lower initialization and measurement fidelity for the active feedback mode-based GST compared to the heralded mode to a combination of an additional leakage probability through S-T_+ anticrossing while preparing (projecting) a state on the $x(z)$ axis of the Bloch sphere and the increased relaxation probability during the idle time between the discrete gates. Nevertheless, these results consolidate the high gate fidelity and low SPAM error illustrating that our Hamiltonian estimation enables the real-time application of general qubit operations in GaAs with the fidelities reaching the level of singlet-triplet qubits in Si devices [46].

In conclusion, using energy-selective tunneling readout-based Hamiltonian parameter estimation of an ST_0 qubit in GaAs, we demonstrated passive and active suppression of nuclear noise, leading to T_2^* above 800 ns, near-ideal quantum oscillation visibility, and gate fidelity up to 99.6% confirmed by both RB and GST comparable with recently demonstrated optimal control-based gate fidelity [47]. The work showcases the improvements in the overall capabilities of GaAs-based spin qubits. With the large SNR of the charge sensor and real-time capability, the EST-based Hamiltonian estimation is potentially useful for advanced quantum control protocols with affordable overhead in classical signal processing, such as error mitigation schemes and entanglement demonstration experiments, where fast qubit parameter calibration with large readout visibility is essential [38].

This work was supported by the Samsung Science and Technology Foundation under Project No. SSTF-BA1502-03. The cryogenic measurement used equipment supported by the National Research Foundation of Korea (NRF) Grant funded by the Korean Government (MSIT) (No. 2018R1A2A3075438, No. 2019M3E4A1080144, No. 2019M3E4A1080145, and No. 2019R1A5A1027055), Korea Basic Science Institute (National Research Facilities and Equipment Center) grant funded by the Ministry of Education (No. 2021R1A6C101B418), and the Creative-Pioneering Researchers Program through Seoul National University (SNU).

*Corresponding author.
dohunkim@snu.ac.kr
†These authors contributed equally to this work.

[1] C. Ferrie, C. Granade, G. Paz-Silva, and H. M. Wiseman, Bayesian quantum noise spectroscopy, New J. Phys. **20**, 123005 (2018).
[2] M. D. Shulman, S. P. Harvey, J. M. Nichol, S. D. Bartlett, A. C. Doherty, V. Umansky, and A. Yacoby, Suppressing qubit dephasing using real-time Hamiltonian estimation, Nat. Commun. **5**, 5156 (2014).
[3] H. Bluhm, S. Foletti, D. Mahalu, V. Umansky, and A. Yacoby, Enhancing the Coherence of a Spin Qubit by Operating it as a Feedback Loop That Controls its Nuclear Spin Bath, Phys. Rev. Lett. **105**, 216803 (2010).
[4] A. Sergeevich, A. Chandran, J. Combes, S. D. Bartlett, and H. M. Wiseman, Characterization of a qubit Hamiltonian using adaptive measurements in a fixed basis, Phys. Rev. A **84**, 052315 (2011).
[5] G. Waldherr, J. Beck, P. Neumann, R. S. Said, M. Nitsche, M. L. Markham, D. J. Twitchen, J. Twamley, F. Jelezko, and J. Wrachtrup, High-dynamic-range magnetometry with a single nuclear spin in diamond, Nat. Nanotechnol. **7**, 105 (2012).
[6] N. M. Nusran, M. U. Momeen, and M. V. G. Dutt, High-dynamic-range magnetometry with a single electronic spin in diamond, Nat. Nanotechnol. **7**, 109 (2012).
[7] T. Nakajima, A. Noiri, K. Kawasaki, J. Yoneda, P. Stano, S. Amaha, T. Otsuka, K. Takeda, M. R. Delbecq, G. Allison, A. Ludwig, A. D. Wieck, D. Loss, and S. Tarucha, Coherence of a Driven Electron Spin Qubit Actively Decoupled from Quasistatic Noise, Phys. Rev. X **10**, 011060 (2020).
[8] M. Veldhorst *et al.*, An addressable quantum dot qubit with fault-tolerant control-fidelity, Nat. Nanotechnol. **9**, 981 (2014).
[9] J. Yoneda *et al.*, A quantum-dot spin qubit with coherence limited by charge noise and fidelity higher than 99.9%, Nat. Nanotechnol. **13**, 102 (2018).
[10] O. E. Dial, M. D. Shulman, S. P. Harvey, H. Bluhm, V. Umansky, and A. Yacoby, Charge Noise Spectroscopy Using Coherent Exchange Oscillations in a Singlet-Triplet Qubit, Phys. Rev. Lett. **110**, 146804 (2013).
[11] J. M. Elzerman, R. Hanson, L. H. W. van Beveren, B. Witkamp, L. M. K. Vandersypen, and L. P. Kouwenhoven, Single-shot read-out of an individual electron spin in a quantum dot, Nature (London) **430**, 431 (2004).
[12] R. Hanson, L. H. W. van Beveren, I. T. Vink, J. M. Elzerman, W. J. M. Naber, F. H. L. Koppens, L. P. Kouwenhoven, and L. M. K. Vandersypen, Single-Shot Readout of Electron Spin States in a Quantum Dot Using Spin-Dependent Tunnel Rates, Phys. Rev. Lett. **94**, 196802 (2005).
[13] J. R. Petta, A. C. Johnson, J. M. Taylor, E. A. Laird, A. Yacoby, M. D. Lukin, C. M. Marcus, M. P. Hanson, and A. C. Gossard, Coherent manipulation of coupled electron spins in semiconductor quantum dots, Science **309**, 2180 (2005).
[14] J. Medford, J. Beil, J. M. Taylor, S. D. Bartlett, A. C. Doherty, E. I. Rashba, D. P. DiVincenzo, H. Lu, A. C. Gossard, and C. M. Marcus, Self-consistent measurement and state tomography of an exchange-only spin qubit, Nat. Nanotechnol. **8**, 654 (2013).

[15] C. Barthel, D. J. Reilly, C. M. Marcus, M. P. Hanson, and A. C. Gossard, Rapid Single-Shot Measurement of a Singlet-Triplet Qubit, Phys. Rev. Lett. **103**, 160503 (2009).
[16] C. Barthel, J. Medford, H. Bluhm, A. Yacoby, C. M. Marcus, M. P. Hanson, and A. C. Gossard, Relaxation and readout visibility of a singlet-triplet qubit in an Overhauser field gradient, Phys. Rev. B **85**, 035306 (2012).
[17] P. Harvey-Collard, B. DAnjou, M. Rudolph, N. T. Jacobson, J. Dominguez, G. A. TenEyck, J. R. Wendt, T. Pluym, M. P. Lilly, W. A. Coish, M. Pioro-Ladriere, and M. S. Carroll, High-Fidelity Single-Shot Readout for a Spin Qubit via an Enhanced Latching Mechanism, Phys. Rev. X **8**, 021046 (2018).
[18] T. Nakajima, M. R. Delbecq, T. Otsuka, P. Stano, S. Amaha, J. Yoneda, A. Noiri, K. Kawasaki, K. Takeda, G. Allison, A. Ludwig, A. D. Wieck, D. Loss, and S. Tarucha, Robust Single-Shot Spin Measurement with 99.5% Fidelity in a Quantum Dot Array, Phys. Rev. Lett. **119**, 017701 (2017).
[19] L. A. Orona, J. M. Nichol, S. P. Harvey, C. G. L. Bottcher, S. Fallahi, G. C. Gardner, M. J. Manfra, and A. Yacoby, Readout of singlet-triplet qubits at large magnetic field gradients, Phys. Rev. B **98**, 125404 (2018).
[20] K. Eng *et al.*, Isotopically enhanced triple-quantum-dot qubit, Sci. Adv. **1**, 7 (2015).
[21] L. A. Tracy, D. R. Luhman, S. M. Carr, N. C. Bishop, G. A. Ten Eyck, T. Pluym, J. R. Wendt, M. P. Lilly, and M. S. Carroll, Single shot spin readout using a cryogenic high-electron-mobility transistor amplifier at sub-Kelvin temperatures, Appl. Phys. Lett. **108**, 063101 (2016).
[22] J. P. Dehollain *et al.*, Optimization of a solid-state electron spin qubit using gate set tomography, New J. Phys. **18**, 103018 (2016).
[23] W. Jang, J. Kim, M. K. Cho, H. Chung, S. Park, J. Eom, V. Umansky, Y. C. Chung, and D. Kim, Robust energy-selective tunneling readout of singlet-triplet qubits under large magnetic field gradient, npj Quantum Inf. **6**, 64 (2020).
[24] D. Keith, M. G. House, M. B. Donnelly, T. F. Watson, B. Weber, and M. Y. Simmons, Single-Shot Spin Readout in Semiconductors Near the Shot-Noise Sensitivity Limit, Phys. Rev. X **9**, 041003 (2019).
[25] D. Keith, S. K. Gorman, L. Kranz, Y. He, J. G. Keizer, M. A. Broome, and M. Y. Simmons, Benchmarking high fidelity single-shot readout of semiconductor qubits, New J. Phys. **21**, 063011 (2019).
[26] See Supplemental Material at http://link.aps.org/supplemental/10.1103/PhysRevLett.129.040501 for details about measurement and FPGA implementation, charge stability diagram and electron temperature, charge sensitivity, visibility analysis, and randomized benchmarking and gate set topography, which includes Refs. [15, 23,24,27–36].
[27] I. Ahmed, A. Chatterjee, S. Barraud, J. J. L. Morton, J. A. Haigh, and M. F. Gonzalez-Zalba, Primary thermometry of a single reservoir using cyclic electron tunneling to a quantum dot, Commun. Phys **1**, 66 (2018).
[28] C. P. Scheller, S. Heizmann, K. Bedner, D. Giss, M. Meschke, D. M. Zumbuhl, J. D. Zimmerman, and A. C. Gossard, Silver-epoxy microwave filters and thermalizers for millikelvin experiments, Appl. Phys. Lett. **104**, 211106 (2014).
[29] J. Stehlik, Y. Y. Liu, C. M. Quintana, C. Eichler, T. R. Hartke, and J. R. Petta, Fast Charge Sensing of a Cavity-Coupled Double Quantum Dot Using a Josephson Parametric Amplifier, Phys. Rev. Applied **4**, 014018 (2015).
[30] Y. Makhlin, G. Schon, and A. Shnirman, Quantum-state engineering with Josephson-junction devices, Rev. Mod. Phys. **73**, 357 (2001).
[31] C. Barthel, M. Kjaergaard, J. Medford, M. Stopa, C. M. Marcus, M. P. Hanson, and A. C. Gossard, Fast sensing of double-dot charge arrangement and spin state with a radio-frequency sensor quantum dot, Phys. Rev. B **81**, 161308(R) (2010).
[32] A. Noiri, K. Takeda, J. Yoneda, T. Nakajima, T. Kodera, and S. Tarucha, Radio-frequency-detected fast charge sensing in undoped silicon quantum dots, Nano Lett. **20**, 947 (2020).
[33] A. Morello *et al.*, Single-shot readout of an electron spin in silicon, Nature (London) **467**, 687 (2010).
[34] R. Blume-Kohout, J. K. Gamble, E. Nielsen, K. Rudinger, J. Mizrahi, K. Fortier, and P. Maunz, Demonstration of qubit operations below a rigorous fault tolerance threshold with gate set tomography, Nat. Commun. **8**, 14485 (2017).
[35] E. Magesan, J. M. Gambetta, B. R. Johnson, C. A. Ryan, J. M. Chow, S. T. Merkel, M. P. daSilva, G. A. Keefe, M. B. Rothwell, T. A. Ohki, M. B. Ketchen, and M. Steffen, Efficient Measurement of Quantum Gate Error by Interleaved Randomized Benchmarking, Phys. Rev. Lett. **109**, 080505 (2012).
[36] E. Nielsen, K. Rudinger, T. Proctor, A. Russo, K. Young, and R. Blume-Kohout, Probing quantum processor performance with pyGSTi, Quantum Sci. Technol. **5**, 044002 (2020).
[37] M. A. I. Johnson, M. T. Mądzik, F. E. Hudson, K. M. Itoh, A. M. Jakob, D. N. Jamieson, A. Dzurak, and A. Morello, Beating the thermal limit of qubit initialization with a Bayesian "Maxwell's demon", arXiv:2110.02046.
[38] J. P. Dehollain*et al.*, Bell's inequality violation with spins in silicon, Nat. Nanotechnol. **11**, 242 (2016).
[39] F. K. Malinowski, F. Martins, L. Cywinski, M. S. Rudner, P. D. Nissen, S. Fallahi, G. C. Gardner, M. J. Manfra, C. M. Marcus, and F. Kuemmeth, Spectrum of the Nuclear Environment for GaAs Spin Qubits, Phys. Rev. Lett. **118**, 177702 (2017).
[40] H. F. Qiao, Y. P. Kandel, K. Y. Deng, S. Fallahi, G. C. Gardner, M. J. Manfra, E. Barnes, and J. M. Nichol, Coherent Multispin Exchange Coupling in a Quantum-Dot Spin Chain, Phys. Rev. X **10**, 031006 (2020).
[41] F. H. L. Koppens, J. A. Folk, J. M. Elzerman, R. Hanson, L. H. Willems van Beveren, I. T. Vink, H. P. Tranitz, W. Wegscheider, L. P. Kouwenhoven, and L. M. K. Vandersypen, Control and detection of singlet-triplet mixing in a random nuclear field, Science **309**, 1346 (2005).
[42] S. Foletti, H. Bluhm, D. Mahalu, V. Umansky, and A. Yacoby, Universal quantum control of two-electron spin quantum bits using dynamic nuclear polarization, Nat. Phys. **5**, 903 (2009).
[43] F. Martins, F. K. Malinowski, P. D. Nissen, E. Barnes, S. Fallahi, G. C. Gardner, M. J. Manfra, C. M. Marcus, and F. Kuemmeth, Noise Suppression Using Symmetric

Exchange Gates in Spin Qubits, Phys. Rev. Lett. **116**, 116801 (2016).

[44] E. Magesan, J. M. Gambetta, and J. Emerson, Scalable and Robust Randomized Benchmarking of Quantum Processes, Phys. Rev. Lett. **106**, 180504 (2011).

[45] E. Magesan, J. M. Gambetta, and J. Emerson, Characterizing quantum gates via randomized benchmarking, Phys. Rev. A **85**, 042311 (2012).

[46] K. Takeda, A. Noiri, J. Yoneda, T. Nakajima, and S. Tarucha, Resonantly Driven Singlet-Triplet Spin Qubit in Silicon, Phys. Rev. Lett. **124**, 117701 (2020).

[47] P. Cerfontaine, T. Botzem, J. Ritzmann, S. S. Humpohl, A. Ludwig, D. Schuh, D. Bougeard, A. D. Wieck, and H. Bluhm, Closed-loop control of a GaAs-based singlet-triplet spin qubit with 99.5% gate fidelity and low leakage, Nat. Commun. **11**, 4144 (2020).